BSc Thesis

Estimating Bridge Surface Temperature with Meteorological And Location Data

By Mahmoud El-Hashash
Supervisor: DR.ING Roland Kromanis
May 6 - July 16 2024

Universiteit Twente
Faculty of Engineering Technology (ET)
Department of Civil ENGineering and Management

Table of Contents

LIST OF FIGURES

List of tables

Preface

"I do not know" are the beautiful words of Malik Ibn Anas, known as Imam Malik, a scholar constantly cited to say these words to questions thrown at him considering his education. This acknowledgement was half of knowledge in his eyes and thus was something he did not shy away from when asked things he had not known with certainty.

I thank my supervisor, Dr.Ing Roland Kromanis, for his patience with me throughout this eye-opening experience and for introducing me to the world of Structural Health Monitoring which helped further my university education to a whole other dimension. The entire process was more iterative than I thought, the more I understood things, the more I understood how much more stands in my way which needs to be learnt.

I thank my sister, whom without I would not have thought critically about my future before applying to university. I thank my brother for all the hours he too invested teaching me previously baffling concepts when I was in this same stage. Equally, they are to be thanked for building my character to what it is today. I thank Professor Lou Bloomfield in the University of Virginia for his series "How things work" that got me interested in engineering. Prior to listening to his spectacularly simple explanations, I ruled it out completely.

I thank my grandmothers for the continuous prayers, which have surely been a reason in my persistence across these challenging 3 years.

Most importantly, I thank God and my wonderful Parents for all I see and do not, without you I would really not know, not a thing at all.

Keywords

Structural Health Monitoring (SHM), open-source modeling, solar radiation, wind speed, bridge surface temperature.

Abstract

Bridges are vital infrastructure elements facing a constant battle against environmental loads and those incurred by daily traffic. One of the most significant environmental effects on bridges is temperature fluctuations. This research investigates current bridge temperature modeling techniques and develops a method to calculate surface temperatures using strictly open-source data with the agenda of increasing both awareness on the effect of temperature on bridges and expanding the knowledge field through open-source tools. In particular, this paper aims to approach the problem of mapping surface temperature across different types of bridges in different locations under one general methodology, away from the FEA methods which provide great accuracy but have a scope limited to a single bridge in the most prominent research works on the matter. A comprehensive understanding of meteorological and environmental factors influencing temperature variations on bridges will thus need to be established, with a particular focus on solar radiation. This is the reigning factor when it comes to computing surface temperature. Both the Perez model and Isotropic model of Liu and Jordan are combined into the methodology. The relative accuracies of these methods are superior to competing diffuse sky models, but the methodology not accounting for conduction skewed results in a negative direction.

1 - Introduction

1.1 The Need for Structural Monitoring

Bridges are critical in facilitating transportation networks, and their failure could lead to catastrophic consequences. Unlike most built structures, bridges are subject to significant stresses from daily traffic loads. These stresses often align with daily recorded peaks of environmental factors such as wind and temperature. Although buildings experience similar environmental variation, bridge spans are constrained by supports at both sides, elements that account for this movement such as expansion joints can not be periodically placed, as they are not supported by the ground compared to other infrastructure.

On notable lengths such as the Danyang-Kunshan Grand Bridge in China 162 kilometers in length (Guinness World Records, 2011) and The Sheikh Jaber Al-Ahmad Al-Sabah Causeway in Kuwait at 48.500 kilometers (SYSTRA, 2020), composed of many of these spans this effect is occurring multiple times throughout the same bridge and these dynamics all converge at once. In comparison, the tallest skyscraper stands at 828 meters (Emaar Properties PJSC, n.d.), highlighting the significant difference in scale between these structures, despite the latter earning much bewonderment from the masses. The holder of the largest bridge span in comparison is 2.023 meters (Cho, 2021) in Turkey. Despite it being more than ten times shorter in overall length than the causeway in Kuwait, since thermal movement scales with length, the aforementioned effect is heightened in the bridge with the larger span.

The Turkish bridge was a reference to the 1915 Çannakale Bridge connecting Europe and Asia. The Kuwaiti bridge forms a connection between a new city being developed and the most dense area in Kuwait in their bid to diversify their economic reliances and expand their talent pool (New Kuwait, n.d.). The Danyang-Kunshan Grand Bridge connected industrial hubs in the workhorse that is China.

The pivotal role bridges play in the provision of accessibility, and so much of recent human development can be attributed to this characteristic; accessibility to knowledge, trade, healthcare etc. Protecting them is of utmost importance. This can also be certainly extended to more humble settings, such as the UT campus footbridge (Marchenko et al., 2024). Although 27 meters in span, it experiences effects not realized in the larger structure like the damage that may be amassed due to temperature gradients from receiving uneven radiation due to shadows (Abid et al., 2022).

Different bridges have different needs across the board to monitor structural health, but remain unified in the need to address these concerns even when considering merely one component such as monitoring temperatures. Due to these unique demands, bridges commonly deploy Structural Health Monitoring (SHM) systems as opposed to buildings.

These systems use sensors to capture details about structural vibrations, which are influenced by traffic loads and environmental factors. Through data analysis and calibration of these vibrations, engineers can assess structure condition and take appropriate management or maintenance measures. Continual monitoring allows for instant detection of weakening or damage, enabling timely repairs to ensure public safety and quality of transportation routes.

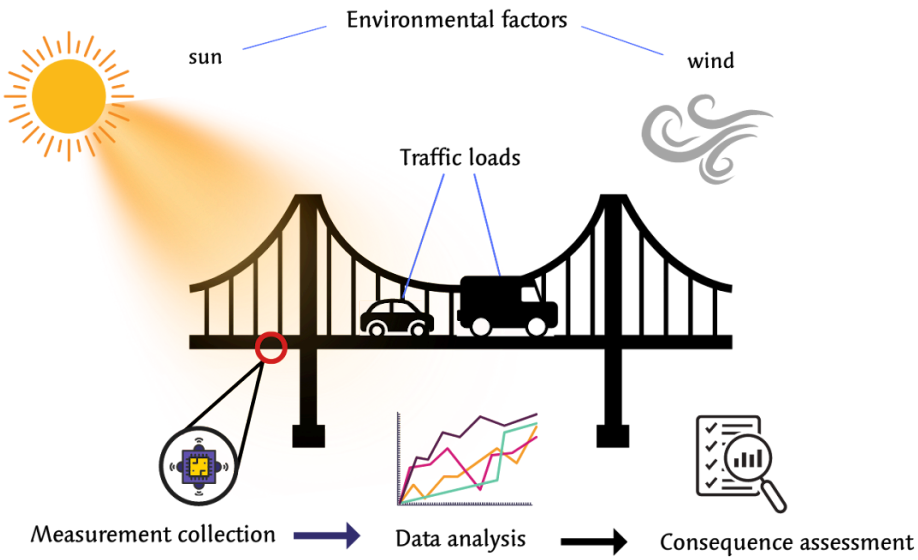

Figure 1: Typical system of a bridge SHM system

Visual inspections, often coupled with non-destructive testing techniques, are traditional methods for assessing bridge conditions. However, these inspections can miss early signs of deterioration, such as deck or cable corrosion (Pines & Aktan, 2002). SHM offers a superior alternative by providing detailed data to enhance visual inspections. Despite their advantages, SHM systems can be costly and complex to install, particularly on older bridges. Carrion et al. (2017) estimated that setting up and maintaining a robust SHM system for 30 years would require 2.12–3.70% of the original bridge cost.

Globally, bridge infrastructure is aging, raising safety and longevity concerns. Taking the example of the United States (US), 46,154 bridges are considered structurally deficient (2021 Infrastructure Report Card). To improve bridge health, proactive maintenance is essential, especially for bridges over 50 years old, which constitute 42.5% of US bridges. The estimated maintenance cost for US bridges is $125 billion (2021

Infrastructure Report Card). Robust SHM systems could have anticipated issues earlier, preventing skyrocketing maintenance costs.

1.2 The Need for Temperature Monitoring

Thermal expansion is usually the first phenomenon that comes to mind when thinking of the aftermath of the interactions of temperature differentials in structures. This effect is measurable and a definite point of concern for bridges (Roeder & Moorty, 1991). Temperature variations throughout the day and year cause both static and dynamic deformations in bridges, sometimes exceeding those induced by traffic (Borah et al., 2021). This necessitates an accurate thermal model to quantify temperature changes' impact on bridge response.

An important concept within diurnal temperature is the lag effect associated with it. Maximum daily temperature does not coincide with maximum solar radiation. It occurs approximately four hours after solar noon, due to a surplus of solar energy in the atmosphere. This surplus causes temperatures to peak in the late afternoon and drop to their lowest before sunrise, emphasizing constant stress fluctuations bridges endure daily. These temperature fluctuations coincide with peak traffic times, creating compounded stress on bridges. Similar to chronic stress in humans, continuous stress fluctuations can have profound impacts on bridge health (McEwen, 2006; Kanner et al., 1981). Thus, temperature monitoring is crucial for maintaining structural health, especially when combined with other stress factors.

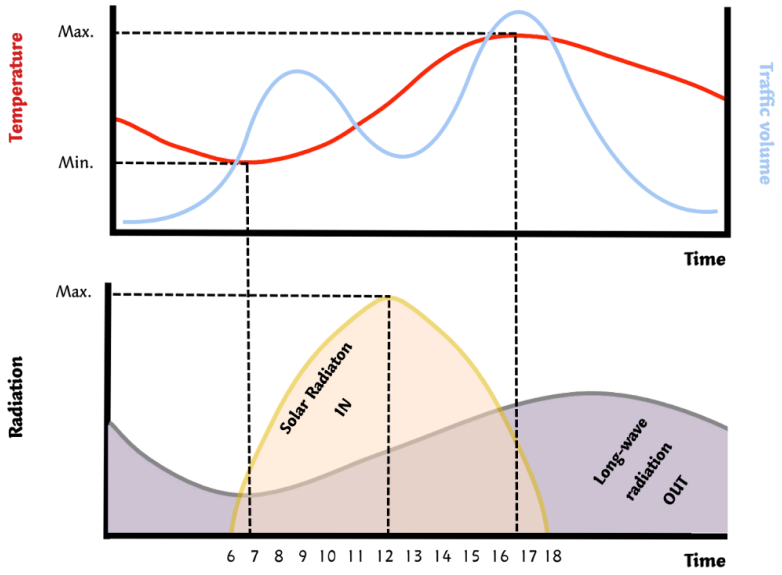

Figure 2: Typical daily trend of temperature, traffic volume and radiation (solar radiation and long wave radiation) for a 12 hour day scenario.

1.3 The Need for General Solutions

This research addresses a significant gap in the existing literature: the lack of general models for estimating bridge surface temperatures. Current models, predominantly Finite Element Analysis (FEA)-based, are tailored to specific bridges, necessitating extensive data collection and computational resources for each individual case. This specificity, while ensuring high precision, limits the broader applicability and scalability of such models. Developing a more general methodology, though potentially less precise, offers substantial benefits.

A generalized model could serve as an approximate indicator of the thermal condition of bridges, providing valuable insights without the need for costly and time-consuming custom models. The integration of Structural Health Monitoring (SHM) data enhances the reliability of this approach by calibrating computational estimates with precise, real-world readings.

The feasibility of a general method is underpinned by the vast and accurate meteorological data available globally via the Internet. To model bridge temperature effectively, it is essential to model the sun's apparent movement and its interaction with the bridge structure, considering any environmental disturbances. Sun path diagrams, which depict the position of the sun relative to a specific location and time, provide a framework for these calculations. By leveraging these diagrams, it is possible to estimate solar radiation on different sides of the bridge, forming the basis for the research conducted in this thesis.

1.4 Research Aim and Objectives

This thesis aims to investigate the validity and accuracy of a computational approach for estimating the surface temperature on the different sides of a bridge using open-source meteorological data and SHM data.

By leveraging available SHM data, the model can utilize sun path data and details of and around the bridge structure to produce and compare realistic temperature values. The research objectives are to:

1- Research literature on relevant alternatives for modeling bridge temperature.

2- Develop a methodology to distinguish between the temperature on each side of a bridge using solar radiation.

3- Integrate environmental disruptors such as wind and shadows into the model to effectively simulate their impact on bridge surface temperatures.

4- Corroborate predicted temperature values using various SHM data sources.

5- Assess critically the flaws of the methodology with sufficient data and reasoning to propose realistic next steps.

1.5 Scope of report

This thesis introduced the topic of focus, thermal analysis, and how that is necessitated by the need for accurate prediction of surface temperatures on bridges to ensure structural integrity and safety. Through this, the formulation of research objectives were possible. Chapter two reviews relevant literature, addressing the first of these objectives. Chapter three details the methodology behind the paper and calculations used to achieve most of its objectives. Chapter four presents the model results using case studies of different bridges, critically assessing the model limitations and positive aspects of it as well. Chapter five concludes with key findings and recommendations for future research.

2 - Literature Review

2.1 The Temperature Effect

A 17-month study of the SHM system at the Corgo bridge in Portugal reported an agreement between most sensors that fluctuations of temperature measurements constituted around 90% of the recorded structural response (Tomé et al., 2018). In their investigation of calculating nonlinear temperature distributions for 26 states, Potgieter and Gamble (1989) found that in clear days, where wind speed is also low, the effect due to temperature can supersede that of traffic. Xia et al. (2012) concludes that frequency variations in civil structures are mainly due to changes in material properties with temperature. In fact, damage is modeled in FE models as black squares representing a loss in stiffness (Posenato et al., 2008), whereas Rishin et al. (1973) established an inversely proportional relationship between temperature and the modulus of elasticity. This is otherwise referred to as Young's modulus and is a measure of material stiffness. From this we can deduce that stress as a result of temperature increase is one of the most significant stresses to a bridge, causing damage through decreasing the stiffness of the material in areas that experience the highest temperature increases.

2.2 The Standard: FEA model

The standard practice when modeling temperature distributions and its effects on a bridge is by adopting a Finite element analysis (FEA) framework. This procedure entails creating a digital replica of the bridge, a digital twin, upon which virtual damage, such as that resulting from thermal loads can be simulated.

In an FEA context, this process is typically executed by projecting radiation onto the structure and delineating the shaded and non-shaded regions. Incorporating the effects of shading and non-shading regions due to radiation onto a structure involves several critical steps, including meshing, applying boundary conditions, conducting shading analysis, configuring the deployed solver, and finally post-processing results and validating the model.

Initially, the structure's geometry is defined and discretized into a finite number of elements through a process called meshing, with the mesh's quality and granularity substantially impacting the analysis' precision. Material properties, including thermal conductivity, density, and specific heat, are assigned to these finite elements.

The governing theory behind such models is mature, with most literature unifying behind a heat transfer model (see Figure 3) applied through a set of boundary conditions that incorporate ingoing short-wave and outgoing long-wave radiation, convection, and conduction effects. The incident radiative flux is modulated based on shading effects, employing various sophisticated methods. Conduction is modeled using the well-established Fourier equation (Fourier, 1878) and convection through Newton’s law

of cooling. The two primary distinctions in the different analyses are in the calculation model of solar radiation and the determination of the convective heat transfer coefficient. These differences are crucial for accurately capturing the thermal behavior of the structure through the transient nature of radiation and convection.

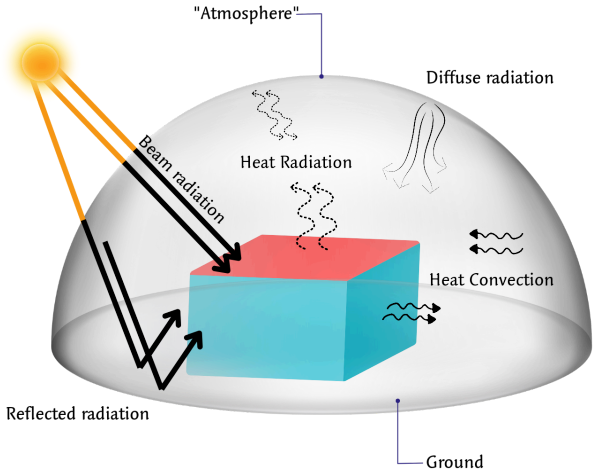

Figure 3: Heat transfer illustrated on a bridge-like structure.

With regards to the differences in literature with the chosen convective heat transfer coefficients, Kehlbeck (1975) developed a set of four empirical formulas to represent the different surfaces of a bridge, including the inner surface for box girders and these are the most widely used equations. Their use is not limited to box girders though (Zhang et al., 2020) and is dictated by the magnitude of wind speed. Other options such as those reported by Jonasson (1994) that are also a function of wind speed but some sources go further, so as to include formulae with surface roughness coefficients (Huang et al., 2022).

Solar radiation encompasses more than just direct solar radiation (Duffie & Beckman, 2013; Wang et al., 2023) and is considered the biggest heat transfer phenomenon in bridges (Tan et al., 2023) thus its consideration must be highly regarded. This radiation has three constituent components: beam, diffuse, and reflected radiation.

The main issue of dispute within the different calculation approaches lies in accounting for diffuse radiation. It can be split into 3 components (Coulson, 1975): isotropic, circumsolar and horizon brightening. Sky models, which describe diffuse radiation, are essential for these calculations. The two leading main models are isotropic and anisotropic diffuse models. The isotropic model (Liu & Jordan, 1963) assumes uniform radiation distribution, leading to underestimations, and is reported to lead to accurate results in cloudy conditions as a result. The anisotropic sky diffuse model aimed to challenge the extent of assumptions made in the isotropic model.

The birth of the coined Hay, Davies, Klucher and Reindl (HDKR) method started to take shape when Klucher (1979) accounted for horizon brightening and added a term for cloudiness through the clearness index to act as a correction to the overestimation caused by Hay and Davies (1980), and this was later backed up by the work of Reindl et al. (1980).

The Perez model (1990) also uses anisotropic principles but extends its complexity by handling brightness coefficients. Despite slight overestimations, the Perez model aligns closely with measured values. The choice between the Perez and HDKR models depends on the bridge orientation (Duffie & Beckman, 2013), although they work best for clear to partly cloudy days.

Tomé et al. (2018) opted for the Isotropic model which helped produce temperature differences below 2°C for most calculated temperatures of the top slab. Consequently, they found the HKDR model not to achieve a higher order of accuracy. Ngo and Nguyen (2024) used HDKR to produce predictive formulae for temperatures on box girders which were in positive agreement with respect to the measured values. Based on this, predictive formulae were extracted for different points on a box girder, enough to understand the different temperature differentials within a cross section. The isotropic model of Liu and Jordan was actually more heavily featured, and showed alignment with measured with average absolute errors produced of 1.1 and maximum absolute errors of 3.2 based on the average of all considered sections (Huang et al., 2022), and in other cases results were slightly lower at 0.9 and 2.2, respectively, for the top and webs (Sheng et al., 2022). They also developed predictive formulae to clarify maximum temperature differences within a vertical cross section.

There is a disproportionality of information with regards to non-clear conditions, in particular, wintery conditions. Even a study in different Canadian climate zones was solely focused on positive thermal gradients (Nassar & Amleh, 2023), although some studies do address such a thing (Ngo and Nguyen, 2024). Tomé et al. (2018) attributed the use of T_{sky}, obtained through empirical equations, instead of the usual T_a, ambient temperature, in the calculation of long wave radiation to the accuracy of his research in capturing wintery conditions. Another change to current heat transfer models is the inclusion of heat flux of evaporation to account for the cooling effect brought on by rain (Görtz et al., 2022).

Subsequently, with the choice of these equations established, radiative heat transfer can be modeled by defining radiation sources, assigning their intensities, and specifying surface properties such as absorptivity, reflectivity, and emissivity, which regulate the interaction of radiation with the material. Shading analysis can then be conducted. FEA methods are commonly used in the realm of modeling temperature through ray-tracing (Zhang et al., 2020), or the hemicube method (Wang et al., 2023). Ray tracing calculates precise paths of the different rays of sunlight as it interacts with the bridge's surfaces, producing realistic shadows and reflections as the sun goes through its daily cycle. The Hemicube method models how sunlight interacts with the surfaces of the bridge and the scene it is in by using a hemicube structure to simulate the distribution of diffuse light.

The FEA solver is then configured for thermal analysis, integrating the effects of conduction, convection, and radiation to resolve the temperature distribution. Post-processing includes analyzing the resultant temperature distributions and corresponding thermal stresses to assess the effects of radiation and shading. Validating the FEA results against experimental data or analytical solutions is essential to quantify and minimize measurement errors, ensuring the model's accuracy and reliability.

Overall, FEA acts as a realistic testbed for the behavior of structures by simulating scenarios that would otherwise not be possible and thus saves time and costs. It can even be used to alter a design to make it more efficient (Cakebread, 2010). It is a powerful tool once sufficiently calibrated, but this power is limited when it comes to widespread implementation due to the data needed for calibration as well as building the models themselves, overall occupying a large amount of computational resources and skills.

Therefore, it would not be an efficient solution to address the gap of global monitoring of bridge health.

3 - Research Methodology

3.1 General Breakdown

The methodology of this research is achieved through the flowchart in Figure 4 and is broken into 5 parts. Firstly, the inputs are addressed. The second part then deals with logic central to the model which deals with deducing when each side of the bridge will be lit via the sun, this is made by obtaining the sun path of the inputted location of the bridge and altering it to remove redundant values per side. The same logic is applied to the wind. From this, solar radiation calculations are set up to finally be able to compute a temperature value once solved. The last step is then taking account of any shadow that may be incident on the bridge, and finding the temperature in that shade. There is a section on error metrics which will be used as a tool to evaluate the predicted temperatures.

The chapter will simply delve into these subjects, also listed on the left side of the flowchart, to detail the calculation process such that the reader can replicate the process. An interesting resource to follow this methodology can also be the Python script that can be accessed in Appendix 7 and perform calculations for you based on your inputs. While the same logic of the methodology is applied, the inputs differ to ease that calculation experience. There is a supporting text with the list of inputs required to be placed or defined within the script. Both the Python script and the calculations in this section are limited to the Northern Hemisphere. It can be applied to the Southern hemisphere but the angles will have to be redefined.

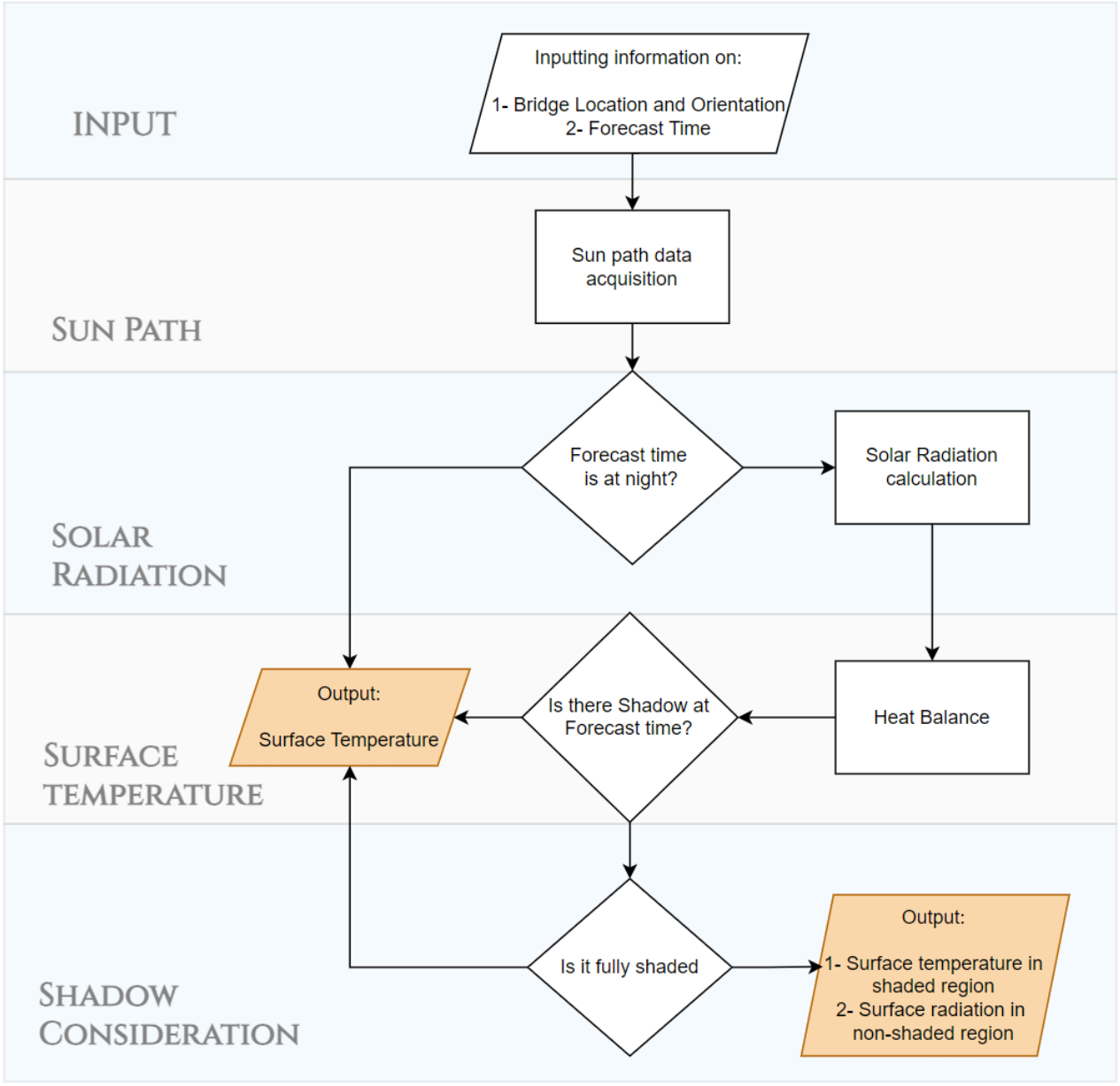

Figure 4: Flowchart depicting methodology.

3.2 Inputs and definitions

Sun path and data on wind speed and direction contextualized to the location of the bridge at a certain time can be either extracted from online sources with the inputs indicating location and time that are listed in Table 1 or even calculated with the help of the angles defined in Table 2.

Table 1: Initial inputs to the model.

Location	Time
Longitude	Day of year (n)
Latitude	Hour of day
Bridge orientation (ob)	

Furthermore, a group of angles and items that dictate the sun path and the succeeding calculations need to be defined to proceed.

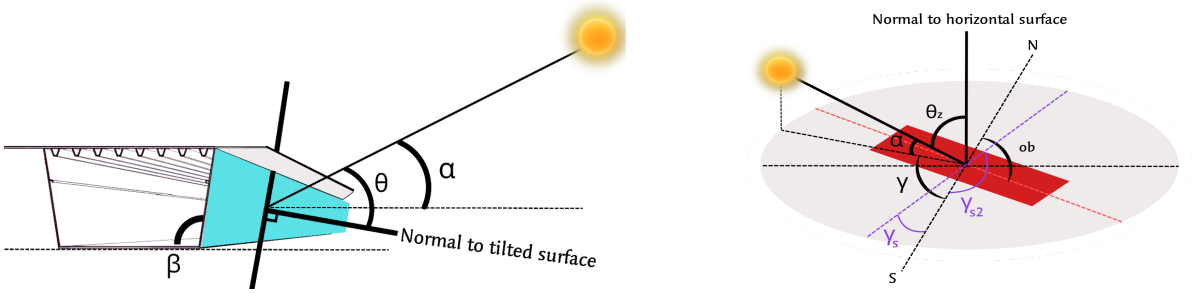

Figure 5: Important angles for the solar radiation calculations.

Table 2 : Important angle descriptions for the solar radiation calculations.

Sign	Angle name	Description
β	Slope	The inclination or steepness of a surface
θ	Angle of Incidence	The angle between a ray of light (or solar radiation) striking a surface and the line perpendicular (normal) to that surface.
γ	Solar Azimuth angle	The compass direction from which sunlight arrives at a horizontal plane, measured clockwise from south in degrees
α	Solar Altitude angle	The angle between the sun's rays and the horizontal plane, measured from the horizon (0° at sunrise/sunset to 90° at zenith).
ob	Bridge orientation	The compass direction in which a bridge is aligned or oriented, indicated by degrees relative to true north.
γ_s	Surface azimuth	The angle between a surface normal and true south, measured clockwise from south, measured on the horizontal plane. Sometimes this is referred to without the s subset. This is another measure bridge orientation, that distinguishes between both webs of the bridge, TN, the north-facing side, and TS, the south-facing side

3.3 Sun Path and Wind

Now, the sun path relevant to that location for a particular day can be tabulated by gathering 3 pieces of information: time, solar altitude angle at that time and the corresponding solar azimuth angle. As any yearly changes are negligible and not accounted for in the calculations, online sources are used for this task. This is done in order to reduce computation time of the process, and thus be able to incorporate a high breadth of data.

This is used to analyze when the bridge should be incident with light, assuming all obstacles such as large towers and trees are not present. Doing so will yield the inequalities presented below and supported by Figure 6 that dictate when the sun is incident on a certain part of the bridge for every orientation.

The north-facing web(TN) is incident with solar radiation when:

$$0 \leq \gamma < ob \tag{1}$$

$$180+ob \leq \gamma \leq 360 \tag{2}$$

The south-facing web (TS) is incident with solar radiation when:

$$ob \leq \gamma < 180+ob \tag{3}$$

As for the top face, it is considered to always be incident with direct solar radiation, which is the opposite of the bottom face.

To model wind, the principle is identical. Wind forecasts in their different forms frequently indicate a compass direction, and the key information with this is that the direction suggests where the wind is originating from. Therefore, translating these compass directions into angles creates the equivalent of an azimuth angle for the wind (d_wind), as it informs on the angle the sun arrives from, and moreover naturally forms the parallel of wind speed with solar radiation.

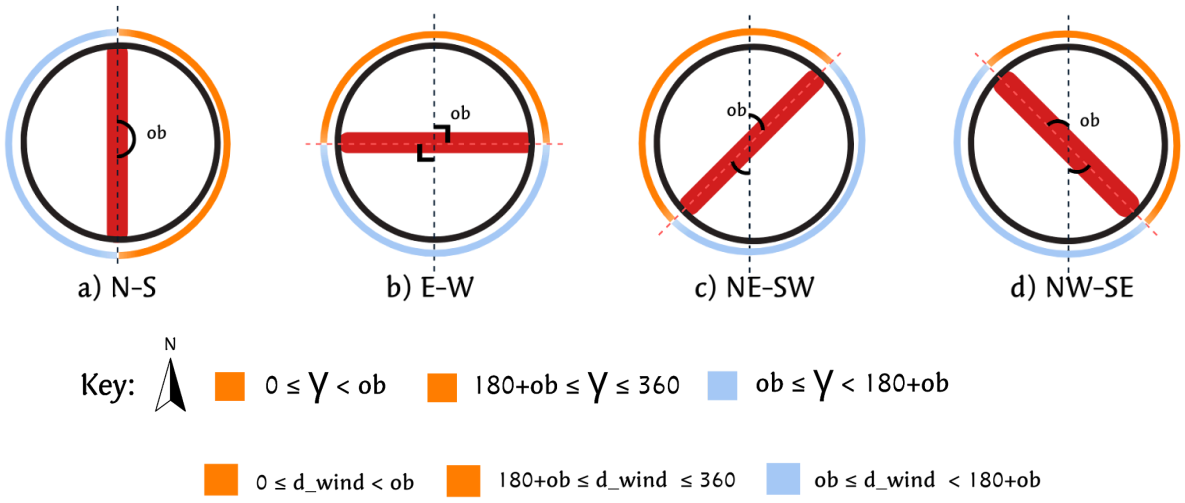

Figure 6: Solar azimuth angles where sun and wind take effect on TN and TS.

When the azimuth angle at the chosen time for the solar radiation calculations for each side is out of the range where the sun is incident, these will be considered to be without beam radiation.

3.4 Solar Radiation

3.41 Calculating solar radiation on horizontal surfaces.

The horizontal surfaces of the bridge are composed of the top slab and what exists of pavement above it. For these surfaces, measurements from solar collectors will definitely supersede empirical formulae in accuracy, but the latter offer a relatively good degree of accuracy to proceed with calculations. The solar radiation will be approximated according to the following equation proposed by Hargreaves and Samani (1982):

$$H = H_0(k_R)\sqrt{(T_{\max} - T_{\min})} \tag{4}$$

Where the factor, k_R, is a geographical factor that should take one of two values. A value of 0.19 should be assigned to bridges with a location in the vicinity of water bodies, and 0.16 if this is not the case. T_max is maximum temperature in the day, T_minobvioudly being the minimum, As for the extraterrestrial radiation, H_0, this refers to the maximum amount of solar radiation that could potentially reach the Earth's surface, disregarding atmospheric effects. A formula to calculate this for a given day is given below :

$$H_o = \frac{24 \times 3600 G_{sc}}{\pi}\left(1 + 0.033\cos\frac{360n}{365}\right) \times \left(\cos\phi\cos\delta\sin\omega_s + \frac{\pi\omega_s}{180}\sin\phi\sin\delta\right) \tag{5}$$

Where G_{SC} is the solar constant, ϕ is latitude, δ is the declination and ω_s is the sunset hour angle, n is the day within the calendar year. With the above information and Appendix 2, a value for H, the total daily radiation, can now be obtained. Using the formula reported by Liu and Jordan (1960) a value for I, the hourly total radiation value, can be estimated once the ratio of hourly to daily radiation, r_t, is obtained from the graph below.

$$r_t = \frac{I}{H} \tag{6}$$

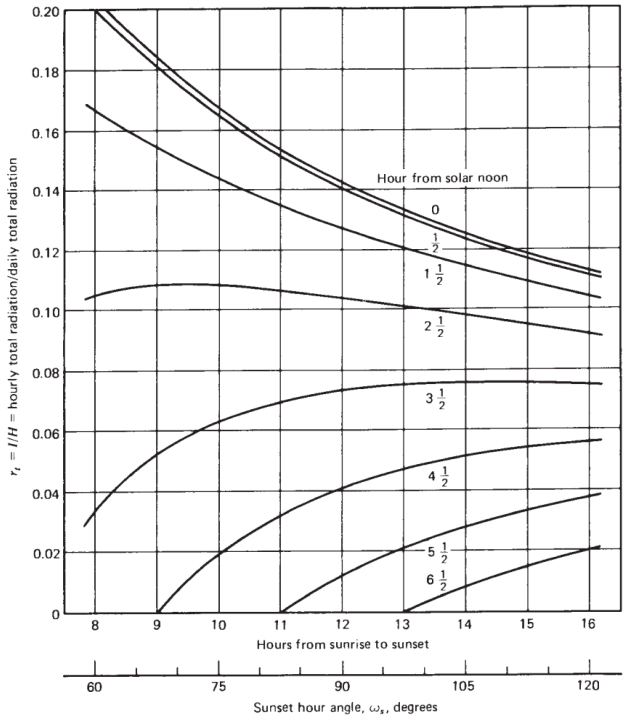

Figure 7: Graph to extrapolate r_t reported by Duffie & Beckman (2013).

3.42 Calculating solar radiation on tilted surfaces.

For tilted surfaces, two methods will be used to take advantage of the strengths of each. Both will be used to obtain the radiation incident on the webs of the bridge girders through the equation for radiation on tilted surfaces, I_T. The Perez method is distinguished between other methods, anisotropic or isotropic, through an extended calculation of brightness and that involves a lengthier calculator process than the others. The Liu and Jordan method, even though way more simplistic in calculation and assumptions, is highly regarded in the bridge temperature monitoring community. In both cases, the hourly total radiation calculated for horizontal surfaces in the calculations tis used and naturally both equations are looked at as three components but the difference lies only in the diffuse portion:

- Beam radiation, I_b,
- Diffuse radiation, I_d,
- Ground reflected radiation, I_g .

The Liu and Jordan method will be used in landscapes regarded as mostly cloudy or overcast as only counting for the isotropic fraction of diffuse causes underestimates making it suitable for situations where not too much variation is expected. However, Perez et al. (1990) meticulously regard horizon brightening and circumsolar diffuse, thus pushing the scale the opposite side and causing overestimates, although slight in nature. Combining both methods could perhaps catch a higher degree of variability not otherwise possible individually.

The Liu and Jordan (1960) simplified a previous isotropic methodology from German compatriots, with the diffuse component in the middle qualifying the isotropic assumption:

$$I_T = I_b R_b + I_d \left(\frac{1 + \cos \beta}{2} \right) + I \rho_g \left(\frac{1 - \cos \beta}{2} \right) \tag{7}$$

Where I_b is the horizontal beam radiation, R_b is the ratio of the cosine of the angle of incidence over the cosine of the zenith angle used to convert I_b to its corresponding value on a tilted surface based on the incidence. ρ_g is commonly referred to as albedo, measuring the reflective quality of surrounding ground.

Perez uses those last terms mentioned, but also incorporates brightness coefficients like F1 and F2 which themselves depend on parameters describing brightness and clearness, of which the equations of can be found in Appendix 4.

$$I_T = I_b R_b + I_d \, (1 - F_1) \left(\frac{1 + \cos \beta}{2} \right) + I_d F_1 \, \frac{a}{b} + I_d F_2 \, \sin \beta + I \rho_g \left(\frac{1 - \cos \beta}{2} \right) \tag{8}$$

3.5 Surface Temperature

3.51 Heat Balance

To accurately calculate the temperature of the bridge surfaces, we employ the heat balance method which incorporates the factors within Figure 3. This approach involves calculating the incoming and outgoing heat on the bridge surfaces and numerically solving for T_s, the surface temperature.

The primary source of incoming heat is solar radiation, Q_S, can be calculated using Solar radiation, I, classified also as short-wave radiation, which is absorbed by the bridge surface and contributes to heating it. This is executed through the following equation:

$$Q_s = \alpha * (I/3600) \quad (9)$$

Where α refers to the short-wave absorptivity of the bridge material.

As for outgoing heat from the bridge surface, two are considered:

1. Long-Wave Radiation: The bridge surface emits energy as long-wave radiation and by assuming it to be a blackbody, the radiative heat loss can be expressed as:

$$Q_r = \sigma * \epsilon_b * (T_s - T_A) \quad (10)$$

where σ is the Stefan-Boltzmann constant at $5.670\times10-8\ Wm^{-2}K^{-4}$, T_A is the ambient temperature, in Kelvin, and T_s is the surface temperature, also in Kelvin, while ϵ_b refers to the emissivity of the material.

2. Convective Heat Loss **:** Wind affects the bridge through forced convection, which can be represented as:

$$Q_c = h_c * (T_s - T_A) \tag{11}$$

where h_c is a heat transfer coefficient which accounts for wind speed.

The Kehlbeck (1975) formulae are used for computing the heat transfer coefficient found below for the different surfaces of the bridge:

$$h_c = \begin{cases} 3.83v + 4.67 & \text{top surface} \\ 3.83v + 2.17 & \text{bottom surface} \\ 3.83v + 3.67 & \text{lateral surface} \\ 3.5 & \text{internal surface} \end{cases} \tag{12}$$

Finally, to determine the surface temperature, we set up the energy balance equation where the incoming energy equals the outgoing energy and numerically solve the equation for T_s :

$$Q_s = Q_r + Q_c \tag{13}$$

3.52 Night-time

This last scenario addresses temperature at night time. In these instances, a thermal coefficient is applied to the ambient temperature. This coefficient adjusts for the absence of additional radiant heat from direct sunlight, based on the fact that temperature forecasts and measurements are typically taken in shaded areas (Mersereau, 2016), and at nighttime it is effectively shade from the sun for a certain number of hours.. The coefficient will be found empirically through the SHM data we will use to obtain the results of the methodology as a whole to accurately reflect these situations. Moreover, we also compute the temperature at the bridge soffit or bottom surface with this same underlying concept. The equation demonstrating this is:

$$T_{s_c} = N_s * T_{a_c} \tag{14}$$

Where T_{s_c} and T_{a_c} are the surface temperature and ambient temperature, in degrees Celsius, and N_s is a correcting coefficient N of side s that can be found in Eq. 21-23 in Chapter 4.

3.6 Shadow consideration

The standard treatment of areas under shadow is to be considered without the beam radiation component. In bridges with short spans, this is a crucial environmental obstacle to consider due to the density of nearby buildings and trees that would cause large parts of the bridge to be obstructed from the incoming solar radiation. An area the model could be very useful in, is identifying the temperature difference in a situation where only certain areas of the bridge are directly radiated on a daily basis. Two temperature values should be computed in that region:

1- A temperature for the lit-up areas using beam and diffuse radiation components

2- A reduced version for the temperature using only diffuse (and reflected radiation)

In the case the entire side is under shade, but should in theory be under the influence of direct solar radiation according to Figure 6, one temperature value should be calculated for the region with the reduced version of solar radiation containing only diffuse and reflected components.

Quantifying the shadow is also essential to capture the relationship of solar radiation with the bridge. In fact, FEA methodologies excel in accuracy due to their in-depth recognition of this. Applications have been developed that overlay shadow on a map for a given time and location, pictures can be extracted to ascertain fractions that determine the external shadow falling upon the bridge.

As for the webs, internal shadow could also be present as a result of the overhang from the top slab (Zhang et al., 2020). Shadow quantification in that case is defined by the following mathematical expressions:

$$is_{web} = \frac{l_{overhang} * tan(\alpha)}{sin(\frac{\pi}{2} + \gamma_s - \gamma) * sin(\beta) - cos(\beta) * tan(\alpha)} \quad (15)$$

$$is_{bot} = \frac{is_{bot} * h_{web}}{tan(\alpha)} \quad (16)$$

Where is_{web} is the internal shadow caused on the web of the girder, is_{bot} the internal shadow on the bottom flange, $l_{overhang}$ the length of the cantilever overhang and h_{web} the height of the web.

3.7 Error metrics

The following metrics are used to judge between measured the suitability between measured SHM values, y_i , and estimated values retrieved from the above methodology, $\hat{y}_i$. In each of the equations below *i* represents the individual data point within the dataset with total data points of *n*.

The Average Absolute Error (AAE) measures the average of the absolute differences between the measured and estimated values. A realistic ideal range would be between 0-1.5.

$$\mathrm{AAE} = \frac{1}{n}\sum_{i=1}^{n}|y_i - \hat{y}_i| \tag{17}$$

The Maximum Absolute Error (MAE) measures the maximum of those same absolute differences between the measured and estimated values. A realistic ideal range would be between 0-2.5.

$$\mathrm{MAE} = \max\left(|y_i - \hat{y}_i|\right) \quad \text{for} \quad i = 1, 2, \ldots, n \tag{18}$$

The Root Mean Square Error (RMSE) measures the average of the squared differences between the measured and estimated values. Since the differences are squared, it provides

a measure of estimation accuracy that is more susceptible to emphasize larger errors. A realistic ideal range would be between 0-2.

$$\mathrm{RMSE} = \sqrt{\frac{1}{n}\sum_{i=1}^{n}(y_i - \hat{y}_i)^2} \tag{19}$$

The Coefficient of Determination (R^2) measures the average of the proportion of the variance in the measured data that is explained by the model, and can be considered a measure of fit . The closer to 1, the better, the more fitting.

$$R^2 = 1 - \frac{\sum_{i=1}^{n}(y_i - \hat{y}_i)^2}{\sum_{i=1}^{n}(y_i - \bar{y})^2} \tag{20}$$

4 - Results and Discussion

4.1 Case studies

Presentation of the results will be done via case studies, where the surface temperature of two bridges will be calculated, testing the veracity of the methodology with the Perez sky. For this, SHM data from the Cleddau Bridge (Kromanis, 2015) and the bridge at the University of Twente (Marchenko et al., 2024) will be used. The selected bridges are different in appearance, characteristics, girder type and function and thus in their loading, including but not exclusive to thermal loads. They retain similarity in orientation, NW-SE, and location with one in Wales and the other Netherlands.

4.11 Cleddau Bridge

The Cleddau Bridge (CB) has an unwanted history of notoriety following its collapse over 50 years ago due to the omission of diaphragms in the design of its box girders. This historical event glorifies the importance of meticulous structural health monitoring, which remains crucial for the bridge's integrity today. Analyzing temperature distribution on bridge surfaces provides insights into potential structural stresses and aids in the necessary philosophy of preventive maintenance.

As depicted in Figure 8, which illustrates temperature data from a hot spring day in 2013, the bottom surface temperatures remain as expected and closely approximate ambient conditions per N_B(Eq. 23), consistently shielded from direct sunlight (Mersereau, 2016). However, significant challenges arise in estimating temperatures on the top and

tilted surfaces. The curve representing the top surface temperature closely mirrors the measured trajectory but is notably shifted approximately 90° leftward on a sinusoidal curve. This displacement causes the estimated and measured values to diverge, resulting in significant deviations as quantified by the statistical metrics calculated in (Eq. 17-20).

Temperature estimation on the bridge webs presents further complications, contributing to the elevated MAE observed. These discrepancies are not confined to sunny days alone but manifest consistently across various conditions as is in the next example. An MAE approaching the AAE aligns closely with findings from FEA studies, where typical AAE values range from 1 to 2 and MAE from 2 to 3. Larger errors of this nature are particularly pronounced during sunrise and sunset periods.

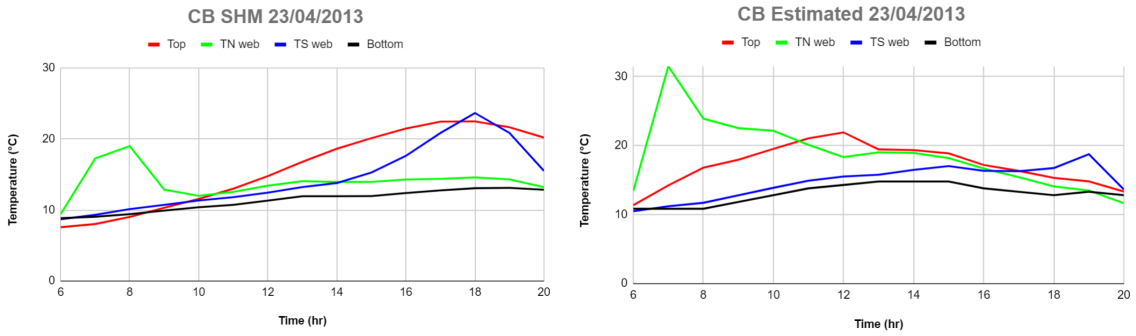

(i) *(ii)*

Figure 8: Cleddau Bridge temperatures on 23/04/13 with (i) measured data and (ii) estimated data

Table 3: Error resulting from use of Perez model with Cleddau Bridge data

AAE	*MAE*	*RMSE*	R^2
3.25	10.49	4.33	0.489

Despite selecting the isotropic model for its known suitability under cloudy conditions, the observed discrepancy between the estimated and measured temperature data reveals a puzzling trend. The isotropic model predicts temperatures that suggest a transition from sunny to more cloudy conditions throughout the day, characterized by initial warmth followed by cooling. However, the SHM data consistently indicates overcast conditions with temperatures remaining stable and tight to ambient levels across all sides of the bridge throughout the day.

This divergence suggests that external factors affecting radiation calculations before entering the isotropic model equations may play a significant role. These factors could include inaccuracies in how solar radiation is assessed or modeled prior to its application in the isotropic equations. Despite these discrepancies, the Coefficient of Determination of 0.515 suggests that the isotropic model explains about 51.5% of the variance in the observed temperature data, indicating a moderate level of predictive capability.

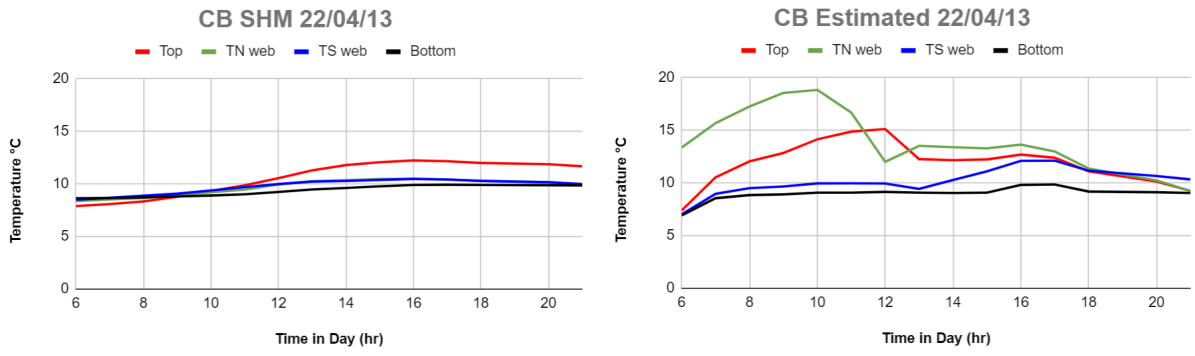

(i) *(ii)*

Figure 9: Cleddau Bridge temperatures on 22/04/13 with (i) measured data and (ii) estimated data

Table 4: Error resulting from use of the Isotropic model with Cleddau Bridge data

AAE	*MAE*	*RMSE*	R^2
2.546	5.67	3.135	0.515

The above mainly concentrated on the relationship between the models and daytime temperature variations. However, capturing general temperature behavior during nighttime is also essential for a complete picture. Using SHM data, coefficients were produced to link nighttime temperatures with ambient temperatures, as solar radiation is not a factor during this period. These coefficients were all close to 1, indicating a strong correlation, with the BLK model consistently showing a coefficient of 1.

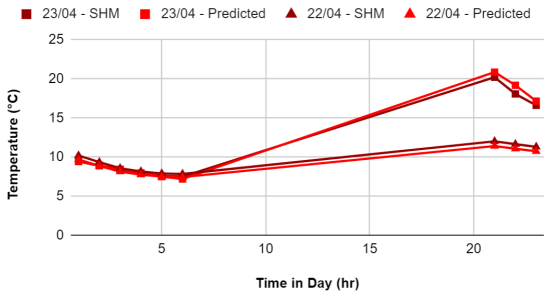

(i)

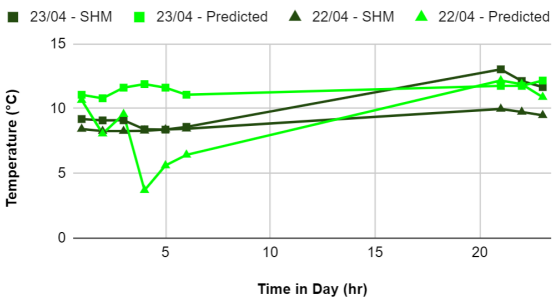

(ii)

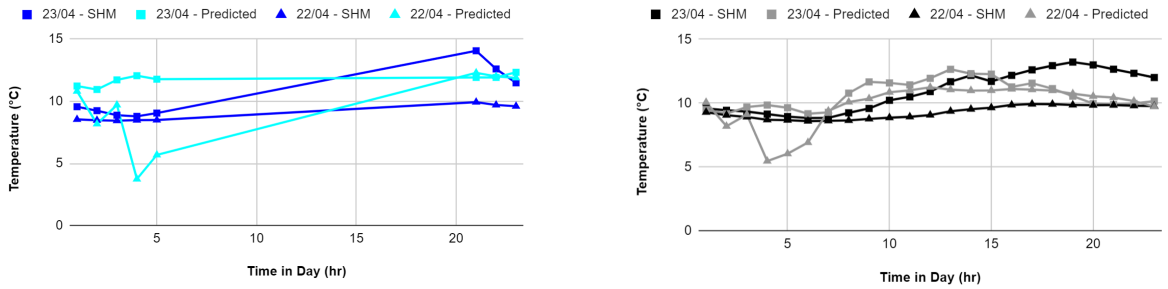

(iii) *(iv)*

Figure 10: Night time temperature coefficients for (i) N_H (ii) N_{TN} (iii) N_{TS} and (iv) N_B

$$N_H = 0.95 \tag{21}$$

$$N_{TN} = N_{TS} = 1.37 \tag{22}$$

$$N_B = 0.99 \approx 1 \tag{23}$$

4.12 University of Twente Footbridge

The University of Twente Bridge (UTB) is situated in Enschede, Netherlands, precisely at coordinates 52.24458 latitude and 6.85458 longitude, with an altitude of approximately 29.1 meters above sea level. The bridge structure consists of three IPE-600 beams and is surrounded by nearby trees and buildings that significantly obstruct direct solar radiation transmission to its top surfaces and webs. This shading effect distinguishes it from structures like the Cleddau Bridge, which benefits from a clear separation from surrounding buildings and trees due to its greater length.

Data was collected using ten sensors placed on the outer bottom flanges of each I-girder, synchronized to monitor web temperatures alternately. Analysis of the data from a clear day, such as June 26, 2024, suggests that the sensors predominantly capture readings in shaded conditions. While temperatures on the TN (north-facing) web remain within acceptable limits, the TS (south-facing) web exhibits notably higher MAE. This discrepancy can be attributed to the bridge's near east-west orientation, exposing the TS web to prolonged solar exposure throughout the day. This observation aligns with the general temperature decrease on the TN web after 10 AM, juxtaposed with an increase in temperature on the TS web.

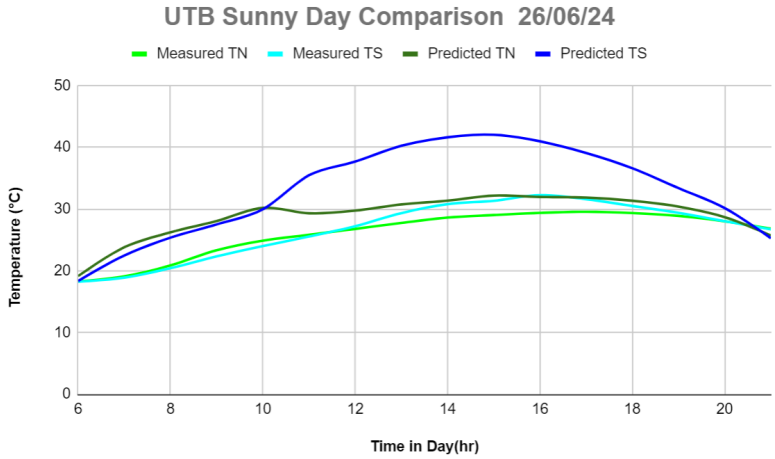

Figure 11: UTB temperatures on 26/06/24 with measured data and predicted data

Table 5: Error resulting from use of Perez model with UTB SHM data

AAE	*MAE*	*RMSE*	R^2
3.86	10.56	4.65	0.44

While sensor data is unavailable for the bottom of the girder and the top surface of the bridge, predictions can be inferred.

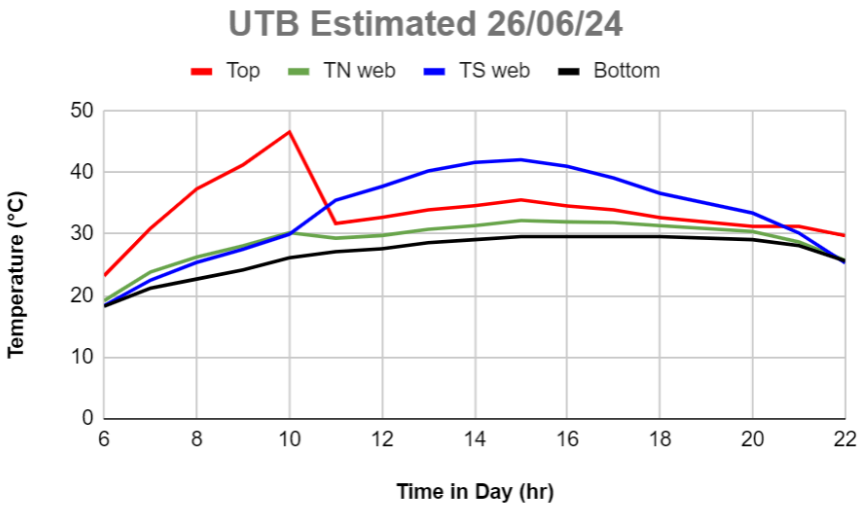

Figure 12: UTB temperatures in the day of 26/06/24 with estimated data

Throughout the day, Figure 12 shows a fairly uniform shape is shared between all the sides of the bridges which is not characteristic of a sunny day, which demonstrates the magnitude of shadow upon the bridge throughout the day. The methodology involves calculating temperatures first, followed by shadow distribution, ensuring accurate assessment where shadows are anticipated. At 10 AM, a distinct temperature peak is observed on the top surface, resulting in a 16°C temperature differential. Moreover, a 6°C temperature variation is noted on the TN side, underscoring the bridge's monitoring necessity.

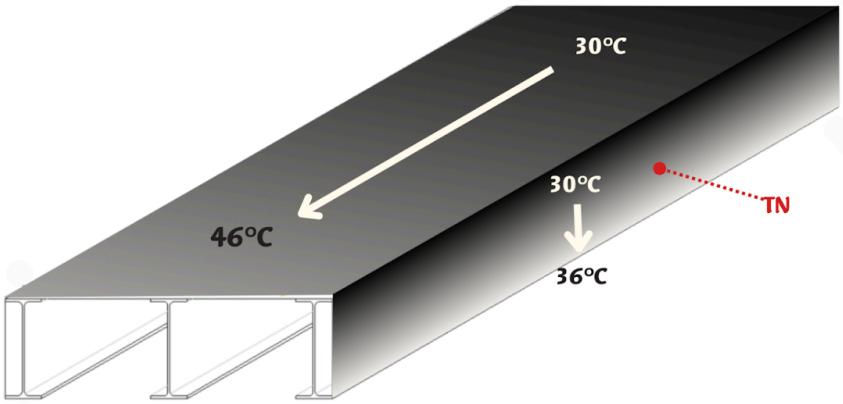

Figure 13: Temperature differences due to shadow on the outer surfaces of the bridge at 10am on 26/06/24 for UTB. Adapted from Marchenko et al. (2024)

4.2 Discussion

4.21 Other diffuse sky models

The poor fit between the estimated and measured temperatures, as highlighted by the inadequate error metrics, calls into question the suitability of the chosen sky models. Extended testing was undertaken to respond to that call through the consideration of other models. The Perez model exhibited relatively superior performance in roughly capturing dynamic radiation changes. Conversely, the isotropic model, known for its conservative nature, often predicted temperatures closer to ambient levels than other models, thereby skewing several estimations in its favor. Simultaneously, evaluations were conducted to measure total horizontal radiation using the Hargreaves and Samani (1982) approximation and averages of radiation data spanning 15 years obtained from PVGIS-SARAH2. Discrepancies between the calculated values from the isotropic, Klucher, HDKR, and Perez models and the actual measured data are detailed through specific error metrics presented below.

Table 6: Average error metrics for two different ways to obtain total horizontal radiation based on Appendix 5

Hargreaves and Samani				Typical Meteorological year			
AAE	MAE	RMSE	R**2	AAE	MAE	RMSE	R**2
3.2	5.9	3.8	0.046	5.5	11	6.4	0.044

Table 7: Average error metrics for four different diffuse sky models based on Appendix 6

	Hargreaves and Samani				Typical Meteorological year			
	AAE	MAE	RMSE	R**2	AAE	MAE	RMSE	R**2
Liu and Jordan	3.2	7.6	4	0.42	4.3	13	5.8	0.3
Klucher	3.6	8.3	4.5	0.38	4.7	14	6.4	0.31
HDKR	3.1	8.2	4.1	0.45	4.4	15	6.3	0.31
Perez	3.7	11	4.9	0.54	4.1	16	6.5	0.42

Despite the relative performance of these models, they all demonstrate inaccuracies to varying degrees. Given that these models are established and generally reliable, it can be ascertained that the issue lies not within the models themselves but rather in their application.

4.22 Conduction

A potential source of error could be the heat balance equation constructed to output the temperatures. Initially, conduction was excluded from the heat balance due to the assumption that surface temperatures did not require its inclusion. The exclusion of conduction from the initial heat balance equation was reasoned based on the understanding that surface temperatures primarily respond to solar radiation and longwave radiation exchanges, which are dominant during daylight hours. Conduction,

which governs heat transfer within materials, typically becomes more significant in scenarios involving temperature gradients and when the external environmental conditions stabilize. For surfaces exposed to direct sunlight, the rapid and dynamic changes in radiation inputs usually overshadow the slower thermal conduction processes within the material. Hence, under the assumption of steady environmental conditions and uniform solar exposure, conduction was initially deemed less influential compared to radiative heat exchange mechanisms in determining surface temperatures. However, incorporating conduction might address the significant discrepancies between measured and estimated temperatures:

4.22.1 Horizontal Surface Temperature

Visual analysis shows a shift compared to SHM data, resembling a 90-degree phase shift to the left on a sinusoidal curve, causing a mismatch between the estimated and measured temperatures. This implies that the peak temperature estimates do not align temporally with the actual measured peaks, indicating a lag in the thermal response. By incorporating conduction, the model would account for the delay in heat transfer through the material, thereby aligning the estimated temperature curves more closely with the measured data.

4.22.2 Overestimations and Underestimations at Sunrise and Sunset

Anomalous R_b values can be mitigated by implementing a smoothing function or threshold to handle the extreme values occurring when the sun is near the horizon. This

approach would prevent the instability caused by the term with the zenith angle approaching zero. Additionally, these extreme values can be removed during data processing, particularly since they typically occur during sunrise or sunset, making them more predictable and manageable. However, a more significant issue arises when employing numerical methods such as finite difference methods, as these anomalies can propagate and affect subsequent calculations, leading to broader inaccuracies in the model. Essentially, this correction can be seen as a prerequisite to incorporating a mechanism like conduction.

Furthermore, basic machine learning techniques could effectively supplement this process. Machine learning models can be trained on historical SHM data to identify patterns and improve the accuracy of temperature predictions. Techniques such as linear regression or neural networks could be employed with the intention of refining the initial estimates and adjusting for interpreted discrepancies, thereby enhancing the overall model performance.

While the initial models provided a foundation, addressing the highlighted issues through conduction and simplifying it through machine learning will significantly improve the accuracy of surface temperature estimations on the bridge. This comprehensive approach ensures a more reliable prediction model, ultimately contributing to the structural health monitoring and safety of bridges.

5 - Conclusion

This study presented a methodology for predicting bridge temperatures with the minimal input of location and time by calculating a few significant meteorological parameters that dictate the sun's position at a given time relative to the different bridge surfaces. The main aim was to investigate its validity and accuracy. It is certainly a promising methodology as the consistent high errors obtained with the solar radiation methods demonstrated through case studies of the Cleddau and University of Twente campus bridges was verified also to be the case with the other solar radiation methods. This tells us the model is not valid due to certain assumptions made and stresses the necessity of further refinement of the methodology by evaluating these assumptions. The main assumption was not incorporating heat conduction into the heat balance. This was assumed to be an unnecessary factor with concern to surface temperature due to solar radiation being the dominant force and that taking precedence.

5.1 Findings

- The comparison of diffuse sky models (Liu and Jordan, Klucher, HDKR, Perez) consistently revealed notable discrepancies next to measured data, with AAE ranging from 3.1 to 4.7, MAE from 7.6 to 16, RMSE from 4.0 to 6.5, and R^2 values between 0.3 and 0.54, and this seems to occur due to the assumption of no conduction.

- Utilizing the approximation of Hargreaves and Samani (1982) along with empirical correlations instead of using long term averages to obtain hourly solar radiation values yields an AAE, MAE and RMSE that are around 43% lower.
- A significant shift in the temperature curve of the horizontal surface of the bridge indicates a potential time lag effect between solar radiation and temperature changes.
- R_b values showed instability near sunrise and sunset, requiring mitigation strategies to improve estimation reliability.

5.2 Recommendations

Based on the findings, the following recommendations are proposed to enhance surface temperature estimation accuracy:

1. **Integrate Fourier Conduction**: Consider integrating Fourier conduction principles into the heat balance model to capture more comprehensive material thermal properties that extend an impact on solar radiation absorption and temperature dynamics.
2. **Increase Testing Sample and Leverage Machine Learning**: Expand the size of the testing dataset and utilize advanced machine learning techniques to discern intricate repeating patterns and relationships from historical data, thereby enhancing the accuracy of temperature estimates.
3. **Define Limits for** R_B: Establish constraints or thresholds for the R_B factor to mitigate extreme values, especially near sunrise and sunset when the sun's angle

approaches the horizon. Implementing defined limits ensures stability in temperature estimations and reduces variability caused by anomalous $R_B$values.

The hope from addressing these recommendations is in ensuring the flow of more reliable and accessible bridge management and thus an added layer to the safety of people trusting engineers with their lives when crossing a bridge. Future research efforts should focus on implementing these strategies to refine existing models and explore emerging technologies for further improvements.

References

2021 Report Card for America's Infrastructure. (2021). https://infrastructurereportcard.org/wp-content/uploads/2020/12/National_IRC_2021-report-2.pdf

Abid, S. R., Xue, J., Liu, J., Tayşi, N., Liu, Y., Özakça, M., & Briseghella, B. (2022). Temperatures and gradients in concrete Bridges: Experimental, finite element analysis and design. *Structures*, *37*, 960–976. https://doi.org/10.1016/j.istruc.2022.01.070

Borah, S., Al-Habaibeh, A., & Kromanis, R. (2022). Measuring thermal response of bridges using vision-based technologies and lvdts. *Lecture Notes in Civil Engineering*, 496–505. https://doi.org/10.1007/978-3-031-07258-1_51

Borah, S., Al-Habaibeh, A., & Kromanis, R. (2021). The effect of temperature variation on bridges—a literature review. *Springer Proceedings in Energy*, 207–212. https://doi.org/10.1007/978-3-030-63916-7_26

Cakebread, T. (2010). The role of Finite Element Analysis in bridge assessment and Design. *Bridge Maintenance, Safety, Management and Life-Cycle Optimization*, 480–480. https://doi.org/10.1201/b10430-369

Carrión, F. J., Quintana, J. A., & Crespo, S. E. (2017). Techno-economical and practical considerations for SHM Systems. *Journal of Civil Structural Health Monitoring*, *7*(2), 207–215. https://doi.org/10.1007/s13349-017-0215-x

Cho, A. (2021, October 8). World's longest suspension bridge takes shape in Turkey. *Engineering News-Record*.

https://www.enr.com/articles/52535-worlds-longest-suspension-bridge-takes-shape-in-turkey

Clark, L. A. (1983). *Concrete bridge design to BS 5400*. Construction Press.

Coulson, K. L., Solar and Terrestrial Radiation, Academic, New York (1975).

Duffie, J. A., & Beckman, W. A. (2013). *Solar Engineering of Thermal Processes*. John Wiley.

Dwivedi, A.K. (2004). Thermal stresses in concrete box girder bridges [Doctoral dissertation, Indian Institute of Technology Roorkee]. https://tinyurl.com/mv49c6a6

Emaar Properties PJSC. (n.d.). *FACT SHEET - BURJ KHALIFA*. https://www.burjkhalifa.ae/img/FACT-SHEET.pdf

Erbs, D., Klein, S., & Duffie, J. (1982). Estimation of the diffuse radiation fraction for hourly, daily and monthly-average global radiation. *Solar Energy*, *28*(4), 293–302. https://doi.org/10.1016/0038-092x(82)90302-4

Fourier, J. B. J. (1878). The analytical theory of heat by Joseph Fourier ; translated, with notes, by Alexander Freeman ; edited for the Syndics of the University Press. https://doi.org/10.5962/bhl.title.18544

Görtz, J., Jürgensen, J., Stolz, D., Wieprecht, S., & Terheiden, K. (2022). Energy load prediction on structures and buildings-Effect of numerical model complexity on simulation of heat fluxes across the structure/environment interface. Applied Energy, 326, 119981. https://doi.org/10.1016/j.apenergy.2022.119981

Guinness World Records. (2011). Longest Bridge. Guinness World Records. https://www.guinnessworldrecords.com/world-records/longest-bridge

Hargreaves, G. H., & Samani, Z. A. (1982). Estimating potential evapotranspiration. *Journal of the Irrigation and Drainage Division*, *108*(3), 225–230. https://doi.org/10.1061/jrcea4.0001390

Hartsuijker, C., & Welleman, JW. (2007). Engineering mechanics : volume 2: stresses, strains, displacements. Springer.

Hay, J. E. and J. A. Davies, in Proceedings of the First Canadian Solar Radiation Data Workshop (J. E. Hay and T. K. Won, eds.), Ministry of Supply and Services, Toronto, Canada, p. 59 (1980). ''Calculation of the Solar Radiation Incident on an Inclined Surface.''

Housner, G. W., Bergman, L. A., Caughey, T. K., Chassiakos, A. G., Claus, R. O., Masri, S. F., Skelton, R. E., Soong, T. T., Spencer, B. F., & Yao, J. T. (1997). Structural control: Past, present, and future. *Journal of Engineering Mechanics*, *123*(9), 897–971. https://doi.org/10.1061/(asce)0733-9399(1997)123:9(897)

Huang, S., Cai, C., Zou, Y., He, X., & Zhou, T. (2022). Investigation of Temperature Variations and Extreme Temperature Differences for the Corrugated Web Steel Beams under Solar Radiation. *Sensors*, *22*(12), 4557. https://doi.org/10.3390/s22124557

Jonasson, J.-E. (1994). Modelling of temperature, moisture and stresses in young concrete (PhD dissertation, Luleå tekniska universitet). Retrieved from https://urn.kb.se/resolve?urn=urn:nbn:se:ltu:diva-25735

Kanner, A. D., Coyne, J. C., Schaefer, C., & Lazarus, R. S. (1981). Comparison of two modes of stress measurement: daily hassles and uplifts versus major life events. Journal of behavioral medicine, 4(1), 1–39. https://doi.org/10.1007/BF00844845

Kehlbeck, F. (1975). Einfluss der Sonnenstrahlung bei Brückenbauwerken. Werner.

Klucher, T. M., Solar Energy, 23, 111 (1979). ‘‘Evaluating Models to Predict Insolation on Tilted Surfaces.’’

Kromanis, R., Kripakaran, P., & Harvey, B. (2015). Long-term structural health monitoring of the Cleddau bridge: evaluation of quasi-static temperature effects on bearing movements. Structure & Infrastructure Engineering/Structure and Infrastructure Engineering, 12(10), 1342–1355. https://doi.org/10.1080/15732479.2015.1117113

Kromanis, R. (2020). Health monitoring of bridges. In Elsevier eBooks (pp. 369–389). https://doi.org/10.1016/b978-0-12-819946-6.00014-x

Linacre, E. T. (1993). *Climate Data & Resources*. Routledge.

Liu, B. Y. H., & Jordan, R. C. (1960). The Interrelationship and characteristic distribution of direct, diffuse and total solar radiation. *Solar Energy*, *4*(3), 1–19. https://doi.org/10.1016/0038-092x(60)90062-1

Liu, B. Y. H. and R. C. Jordan, Solar Energy, 7, 53 (1963). ‘‘The Long-Term Average Performance of Flat-Plate Solar Energy Collectors.’’

Marchenko, A., Kromanis, R., & Dorée, A. G. (2024). Characterizing bridge thermal response for bridge load rating and condition assessment: A parametric study. *Infrastructures*, *9*(2), 20. https://doi.org/10.3390/infrastructures9020020

McEwen, B. S. (2006). Protective and damaging effects of stress mediators: central role of the brain. Dialogues in Clinical Neuroscience, 8(4), 367–381. https://doi.org/10.31887/dcns.2006.8.4/bmcewen

Mersereau, D. (2016, June 29). *There’s no such thing as “the temperature in the shade.”* MentalFloss.

https://www.mentalfloss.com/article/82406/theres-no-such-thing-temperature-shade

Nassar, M., & Amleh, L. (2023). Transient thermal Analysis of concrete box girders: Assessing temperature variations in Canadian climate zones. *Sensors*, *23*(19), 8206. https://doi.org/10.3390/s23198206

New Kuwait. (n.d.). https://www.newkuwait.gov.kw/plan.aspx

Ngo, D.-Q., & Nguyen, H.-C. (2024). Monitoring and analysis of temperature distribution in reinforced concrete bridge box girders in Vietnam. *Case Studies in Construction Materials*, *20*. https://doi.org/10.1016/j.cscm.2024.e02857

Potgieter, I. C., & Gamble, W. L. (1989). Nonlinear temperature distributions in bridges at different locations in the United States. PCI Journal, 34(4), 80–103. https://doi.org/10.15554/pcij.07011989.80.103

Pines, D., & Aktan, A. E. (2002). Status of structural health monitoring of long-span bridges in the United States. Progress in Structural Engineering and Materials, 4(4), 372–380. https://doi.org/10.1002/pse.129

Page, J. M., & Lebens, R. (1986). Climate in the United Kingdom : a handbook of solar radiation, temperature and other data for thirteen principal cities and towns / edited by John Page and Ralph Lebens. HMSO.

Perez, R., P. Ineichen, R. Seals, J. Michalsky, and R. Stewart, Solar Energy, 44, 271 (1990). ‘‘Modeling Daylight Availability and Irradiance Components from Direct and Global Irradiance.’’

Reindl, D. T., W. A. Beckman, and J. A. Duffie, Solar Energy, 45, 9 (1990b). ‘‘Evaluation of Hourly Tilted Surface Radiation Models.’’

Roeder, C. W., & Moorty, S. (1991). Thermal movements in bridges. *Report for NSF*.

Sheng, X., Zhou, T., Huang, S., Cai, C., & Shi, T. (2022). Prediction of vertical temperature gradient on concrete box-girder considering different locations in China. *Case Studies in Construction Materials*, *16*, e01026. https://doi.org/10.1016/j.cscm.2022.e01026

SYSTRA. (2020, November 23). *Sheikh Jaber Al-Ahmad Al-Sabah causeway – Kuwait - Group*. Group. https://www.systra.com/en/project/subiyah-bridge-kuwait/

Tan, H., Qian, D., Xu, Y., Yuan, M., & Zhao, H. (2023). Analysis of vertical temperature gradients and their effects on hybrid girder cable-stayed bridges. *Sustainability*, *15*(2), 1053. https://doi.org/10.3390/su15021053

Wang, A., Zhang, Z., Lei, X., Xia, Y., & Sun, L. (2021). All-Weather thermal simulation methods for Concrete Maglev Bridge based on structural and meteorological monitoring data. *Sensors*, *21*(17), 5789. https://doi.org/10.3390/s21175789

Wang, Y.-G., He, X.-J., Ouyang, F., He, J., Wu, W.-W., & Wu, C. (2023). New method for fine calculation of bridge temperature field based on BIM solar radiation analysis. *Advances in Civil Engineering*, *2023*, 1–13. https://doi.org/10.1155/2023/6855116

Xia, Y., Chen, B., Weng, S., Ni, Y., & Xu, Y. (2012). Temperature effect on vibration properties of civil structures: a literature review and case studies. *Journal of Civil Structural Health Monitoring*, *2*(1), 29–46. https://doi.org/10.1007/s13349-011-0015-7

Zhang, C., Liu, Y., Liu, J., Yuan, Z., Zhang, G., & Ma, Z. (2020). Validation of long-term temperature simulations in a steel-concrete composite girder. *Structures*, *27*, 1962–1976. https://doi.org/10.1016/j.istruc.2020.07.070

Zhang, G., Wang, B., Li, J., & Xu, Y. (2022). The application of deep learning in bridge health monitoring: a literature review. Advances in Bridge Engineering, 3(1). https://doi.org/10.1186/s43251-022-00078-7

Appendices

These appendices will show anything not made clear in the text such as content of equations beyond what is getting solved, as well as any additional information supporting the text.

Appendix 1 : Hargreaves and Samani (1982) approximation contents

H	H_0	k_R	T_{max}	T_{min}
Solar radiation on horizontal surfaces for day (J/m^2)	Extraterrestrial radiation for day (J/m^2)	Geographical factor	Maximum temperature for day (°C)	Minimum temperature for day (°C)

Appendix 2 : Contents of Equation for daily extraterrestrial radiation

H_0	G_{sc}	n	ϕ	δ	ω_s
Extraterrestrial radiation for day (J/m^2)	Solar constant (W/m^2)	Day of year	Latitude	Declination	Sunset hour angle (°)
	1367 W/m^2			$\delta = 23.45 \sin\left(360 \frac{284+n}{365}\right)$	$\cos \omega_s = -\frac{\sin \phi \sin \delta}{\cos \phi \cos \delta} = -\tan \phi \tan$

Appendix 3: Aid to solve for beam and diffuse radiation using Erbs et al. (1982) correlation

I_b	I_d	R_b	ρ_g
Beam radiation (J/m^2)	Diffuse radiation (J/m^2)	Ratio of beam radiation on a tilted surface	Ground reflectance
$I_b = I - I_d$	$I_d = I - I_b$	$R_b = \frac{G_{b,T}}{G_b} = \frac{G_{b,n}\cos\theta}{G_{b,n}\cos\theta_z} = \frac{\cos\theta}{\cos\theta_z}$	Values by Page & Lebens (1986)

$$\frac{I_d}{I} = \begin{cases} 1.0 - 0.09k_T & \text{for } k_T \le 0.22 \\ 0.9511 - 0.1604k_T + 4.388k_T^2 - 16.638k_T^3 + 12.336k_T^4 & \text{for } 0.22 < k_T \le 0.80 \\ 0.165 & \text{for } k_T > 0.8 \end{cases}$$

$$k_T = \frac{I}{I_o}$$

$$I_o = \frac{12 \times 3600}{\pi} G_{sc}\left(1 + 0.033\cos\frac{360n}{365}\right) \times \left[\cos\phi\cos\delta\left(\sin\omega_2 - \sin\omega_1\right) + \frac{\pi(\omega_2 - \omega_1)}{180}\sin\phi\sin\delta\right]$$

Appendix 4: Equations to solve for Perez et al. (1990) model

$$F_1 = \max\left[0, \left(f_{11} + f_{12}\Delta + \frac{\pi\theta_z}{180} f_{13}\right)\right]$$

$$F_2 = \left(f_{21} + f_{22}\Delta + \frac{\pi\theta_z}{180} f_{23}\right)$$

Where f_{ii} are brightness coefficients and Δ is a brightness parameter

Range of ε	f_{11}	f_{12}	f_{13}	f_{21}	f_{22}	f_{23}
1.000–1.065	−0.008	0.588	−0.062	−0.060	0.072	−0.022
1.065–1.230	0.130	0.683	−0.151	−0.019	0.066	−0.029
1.230–1.500	0.330	0.487	−0.221	0.055	−0.064	−0.026
1.500–1.950	0.568	0.187	−0.295	0.109	−0.152	0.014
1.950–2.800	0.873	−0.392	−0.362	0.226	−0.462	0.001
2.800–4.500	1.132	−1.237	−0.412	0.288	−0.823	0.056
4.500–6.200	1.060	−1.600	−0.359	0.264	−1.127	0.131
6.200–∞	0.678	−0.327	−0.250	0.156	−1.377	0.251

Where ϵ is a clearness parameter

$$\varepsilon = \frac{\frac{I_d + I_{b,n}}{I_d} + 5.535 \times 10^{-6}\,\theta_z^3}{1 + 5.535 \times 10^{-6}\,\theta_z^3}$$

$$I_{b,n} = I_b / \cos\theta_z$$

$$\Delta = m\,\frac{I_d}{I_{on}}$$

$$I_{on} =$$

$$G_{sc}\left(1 + 0.033\cos\frac{360n}{365}\right)$$

$$m = \frac{1}{\cos \theta_z}$$

But when $\theta_z > 70$

$$m = \frac{\exp(-0.0001184h)}{\cos(\theta_z) + 0.5057(96.080 - \theta_z)^{-1.634}}$$

Appendix 5: Error metrics breakdown for two different ways to obtain total horizontal radiation

	Hargreaves and Samani				Typical Meteorological year			
	AAE	MAE	RMSE	R**2	AAE	MAE	RMSE	R**2
Sunny Day	5.6	8.1	6.1	0.0021	7.6	15	8.8	0.1
Mostly Cloudy	2.2	5	2.8	0.013	2.5	5.8	2.9	0.015
Mixed Cloudy and Sunny	1.9	4.8	2.4	0.12	6.3	12	7.4	0.014

Appendix 6: Error metrics breakdown for four different diffuse sky models based

		Hargreaves and Samani				Typical Meteorological year			
		AAE	MAE	RMSE	R**2	AAE	MAE	RMSE	R**2
Liu and Jordan	Sunny Day	3.8	9.1	4.5	0.14	4.1	13	5.5	0.21
	Mostly Cloudy	2.5	5.7	3.1	0.52	2.6	8.6	3.7	0.2
	Mixed Cloudy and Sunny	2.4	7.8	3.5	0.19	3.9	14	6.2	0.39
	Shadowed areas	4.3	8	4.8	0.83	6.5	14	7.8	0.39
Klucher	Sunny Day	4.3	9.6	5.1	0.12	4.8	14	6.2	0.25
	Mostly Cloudy	3.2	6.5	3.7	0.44	2.9	9.1	4.1	0.24
	Mixed Cloudy and Sunny	2.5	8	3.6	0.18	3.6	16	6.2	0.38
	Shadowed areas	4.6	9.1	5.4	0.79	7.5	16	9.1	0.35
HDKR	Sunny Day	3.3	9.6	4.3	0.21	5.2	14	6.3	0.34
	Mostly Cloudy	2.8	7.1	3.7	0.73	2.6	9.9	4.1	0.17
	Mixed Cloudy and Sunny	2.5	8	3.7	0.18	4.4	18	7.4	0.4
	Shadowed areas	3.7	8.2	4.7	0.69	5.4	17	7.5	0.31
Perez	Sunny Day	3.9	11	4.7	0.44	5.4	25	8.8	0.4

	Mostly Cloudy	3.3	12	4.9	0.53	3.2	13	4.8	0.33
	Mixed Cloudy and Sunny	2.6	10	4	0.54	2.9	16	5.9	0.49
	Shadowed areas	5.2	10	6	0.64	5	12	6.4	0.46

Appendix 7: Python Code

BSc_Thesis Python